tained here for $Q(Xe^{129*})$ brings the Mössbauer-effect results on the structure of xenon fluorides into agreement with expectations[23] based on other types of measurement.

ACKNOWLEDGMENTS

The author would like to acknowledge helpful conversations at various times with A. Arima, S. Ruby, H. DeWaard, and P. Stelson. He is indebted to C. Chernick and J. Malm for the XeF_4 sample and to M. R. Perlow for the I^{129} compounds used as sources. He wishes to thank M. H. Mueller and L. R. Heaton for crystallographic examination of an XeF_4 sample and S. Siegel and J. H. Burns for additional crystallographic information. J. Oyler was very helpful in taking and reducing the data, and E. Kolacek and B. Martinka of the machine shops were responsible for the construction of the spectrometer.

[23] D. Lazdins, C. W. Kern, and M. Karplus, J. Chem. Phys. **39**, 1611 (1963).

PHYSICAL REVIEW VOLUME 135, NUMBER 5B 7 SEPTEMBER 1964

Recoil Studies of Nuclear Reactions Induced by High-Energy Particles. I. Production of Tb^{149}†

LESTER WINSBERG*

Argonne National Laboratory, Argonne, Illinois

and

Lawrence Radiation Laboratory, University of California, Berkeley, California

(Received 17 February 1964)

The interaction of high-energy protons and alpha particles with Ta, Au, and Bi to produce Tb^{149} was investigated by the recoil technique and by measuring the excitation functions. The experimental results were analyzed in terms of a two-step mechanism: (1) An initial interaction causes the struck nucleus to recoil forward. (2) This excited nucleus then loses its energy of excitation by emitting various particles until the final nucleus is formed. The results of this analysis confirm the main features of this mechanism. These results were further analyzed for the details of the mechanism by applying the laws of energy and momentum conservation in a general way.

IT is almost axiomatic that one gains the greatest insight into any process by studying it from many points of view. This is particularly true of nuclear reactions where the phenomena are complex and the experimental results difficult to interpret. On the other hand, the number of different types of experiment one can perform in any given investigation are limited. The study reported here was initiated in order to see how much could be learned by applying the simplest techniques to a typical nuclear reaction.

The reaction studied was the production of Tb^{149} from Ta^{181}, Au^{197}, and Bi^{209}. Here, the product is appreciably lighter than the target nucleus. The reactions were initiated by protons and alpha particles with energies above 400 MeV. The maximum proton energy was 6.2 BeV; for alpha particles, 0.88 BeV.

These systems were chosen because the target foils are readily available, and because the ground state of Tb^{149} is an easily identifiable alpha-particle emitter.[1–3] The target foils were exposed to proton beams from the bevatron in Berkeley and the Fermi Institute cyclotron at the University of Chicago and to protons and alpha particles from the 184-in. cyclotron in Berkeley. The excitation functions and recoil properties of the final product, Tb^{149}, were measured.

Thus, we have two types of measurement made over a range of bombarding energies with both protons and alpha particles. This variety of information was essential for revealing some of the salient features of the reaction mechanism given in the Summary.

EXPERIMENTAL PROCEDURE

Two types of experiments were performed: In the first type the target foil [No. 1 in Fig. 1(a)] and the Al catcher foils surrounding them (No. 2) were thick (several mg/cm²) relative to the range of the recoiling Tb^{149}. Several additional $\frac{1}{4}$-mil Al foils were included as cross-section monitors (No. 3). Aluminum cover foils (No. 4) protected the ensemble. The excitation functions are based primarily on data obtained in these experiments. Values of the cross sections obtained in the second type of experiment agree with these values to better than 10%.

In the second type of experiment the targets consisted of thin films (mostly of thickness ~30 μg/cm²) of

† This work was done under the auspices of the U. S. Atomic Energy Commission.

* Present address: The University of Illinois at Chicago Circle, Chicago, Illinois.

[1] J. O. Rasmussen, S. G. Thompson, and A. Ghiorso, Phys. Rev. **89**, 33 (1953).

[2] L. Winsberg, Bull. Am. Phys. Soc. **3**, 406 (1958).

[3] R. D. Macfarlane, Phys. Rev. **126**, 274 (1962).

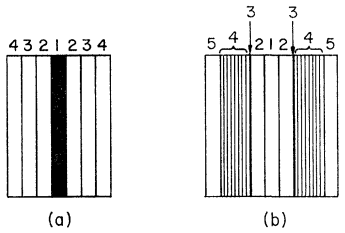

FIG. 1. Composition of foil stacks (a) used for cross-section measurements—foil No. 1, several mg/cm² of Ta, Au, or Bi metal; foil Nos. 2–4, ¼-mil Al; (b) used for recoil measurements—foil Nos. 1 and 5, ¼-mil Al; foil Nos. 2 and 3, thin film of metal (No. 3) evaporated on ¼-mil Al foil (No. 2); foil No. 4, Al leaf (~150 μg/cm²).

Ta, Au, and Bi [No. 3 in Fig. 1(b)], evaporated on ¼-mil Al foil (No. 2). Each foil was cut in two and the parts placed back to back with a ¼-mil Al monitor foil (No. 1) inserted between. On either side of this stack were located up to 10 sheets of Al leaf of thickness ~150 μg/cm² (No. 4). The Al cover foils are marked No. 5. The recoil information is based on this latter type of experiment.

The foil assemblies in both types of experiments were clamped in a holder and oriented either perpendicular to the beam for measuring the forward and backward projections of the recoil range [Fig. 2(a)] or in line with the beam for measuring the perpendicular components [Fig. 2(b)]. After the bombardment, the total alpha activity present in the target foil or recoiling into the adjacent catchers was measured in a set of 8 to 14 ionization chambers. A few hours later, all samples, except those from the alpha-particle bombardment of Bi, decayed with the 4.1-h half-life of Tb^{149}, confirming earlier observations.[1] (The branching ratio for alpha decay of the ground state is approximately 10%.[2] The half-life of the excited state is 4.0 *m*.[3] The branching ratios for various modes of decay of this isomer have not been reported.) The ranges of the Tb^{149} alpha particles in tantalum were determined by comparing the Tb^{149} activity from targets of different thickness which had been irradiated under identical conditions. The ranges in gold and bismuth had been determined previously.[4] The resulting values used to correct for self-absorption in the target are 10.6 mg/cm² in Ta, 11.0 mg/cm² in Au, and 11.4 mg/cm² in Bi. The range in Al was taken to be 3.7 mg/cm².

The bombardment of Bi with alpha particles leads to the production of several alpha-emitting isotopes of At.

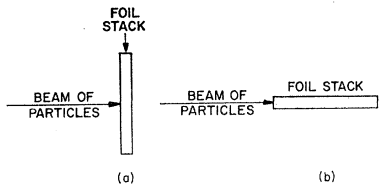

FIG. 2. Orientation of foil stacks for determining (a) forward and backward recoils and (b) perpendicular recoils.

[4] G. Friedlander (private communication).

It was not possible to analyze the resulting decay curves unambiguously into a Tb^{149} component. Hence, this reaction was not studied further.

The results from the thin-target experiments were corrected to a target of zero thickness. This correction increased the amount of activity recoiling backward by several percent and the amount recoiling forward by a lesser amount. The activity in each of the catcher foils was then normalized to a total activity recoiling out of the target equal to unity. The data from these experiments are tabulated in the Appendix. Typical results of such thin-target measurements are shown in differential form in Fig. 3. The ordinate $F(t)/\Delta t$ is the fraction of the total activity found in a given foil divided by the thickness of the foil. The abscissa is the total thickness t.

The experimental cross sections are based on previously determined values for the formation of Na^{24} from Al. The cross sections for this reaction from proton bombardments were taken directly from Table V of Ref. 5 or obtained by interpolation where necessary.

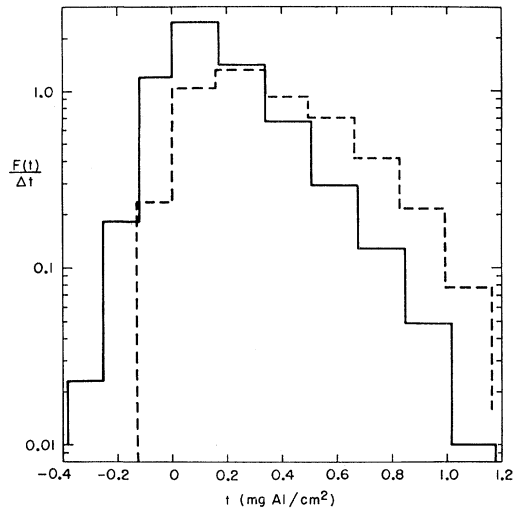

FIG. 3. The range distribution of Tb^{149} from proton (solid line) and alpha-particle (dashed line) bombardments of Ta^{181} at 700 MeV. The forward direction is indicated by positive values of t, the thickness of the Al absorbers. Negative values indicate the backward direction. The ordinate $F(t)/\Delta t$ is the fraction of the total activity found in a given foil divided by the thickness of the foil.

The corresponding cross sections for alpha-particle bombardment have been measured only to 380 MeV.[6] At 500 MeV it is taken to be 22 mb, at 700 MeV, 17 mb, and at 880 MeV, 14 mb, as obtained by extrapolation.

ANALYSIS OF RECOIL DATA

The purpose of this study is to determine the reaction mechanism. In general, it is not possible to get this information directly from the experimental data. The

[5] J. B. Cumming, Ann. Rev. Nucl. Sci. **13**, 261 (1963).
[6] M. Lindner and R. N. Osborne, Phys. Rev. **91**, 342 (1953).

usual procedure is to analyze the data in terms of several models. By means of this comparison, some of the proposed models may be unambiguously rejected. A model that is consistent with the experimental data is useful for determining the values of the various parameters describing the reaction mechanism.

A successful model for describing many nuclear reactions is that in which the incident particle is absorbed to form an excited compound state.[7–9] This compound nucleus has the velocity and momentum of the center of mass, and loses its energy of excitation by means of nuclear evaporation, nuclear fission, or gamma-ray emission. The calculated value of the recoil momentum, p_{CN}, of any intermediate excited nucleus, formed during the course of the de-excitation process, can be compared with the measured value in the forward direction p_{II} of that nucleus. Agreement between these two values is evidence for a compound-nucleus mechanism.

The details of the determination of p_{II} in the reactions studied here are given later. However, the values of p_{II}/p_{CN}, as given in Table IV, unambiguously rule out the compound-nucleus mechanism for any of these reactions. These values range from 0.04 to 0.65. None is close to unity, the value predicted by the compound-nucleus model.

The model that was adopted is a modification of the compound-nucleus mechanism.[10–13] In the first phase of the interaction, the incident particle (p or α) collides with the target nucleus, causing the emission of an undetermined number of particles. An intermediate excited nucleus remains having the velocity **v** and the momentum **p**. As we have just seen, the values of p_{II}, and hence v_{II}, are significantly smaller than the compound-nucleus values. The inclusion of a perpendicular component $v_\perp$ does not affect the results of this analysis appreciably, as will be shown later.

In the second phase, the intermediate excited nucleus emits more particles until Tb^{149} is finally formed. This phase may be pure nuclear evaporation. The analysis merely assumes that the differential cross section of the Tb^{149} recoil is isotropic in the system of the intermediate nucleus. A less stringent assumption, namely symmetry around 90° in this system, is not expected to affect the results of this analysis appreciably. As a result of this second phase the recoiling Tb^{149} atom has acquired an additional isotropically directed velocity **V**. The final velocity vector of the Tb^{149} atom is the vector sum, **v**+**V**, see Fig. 4.

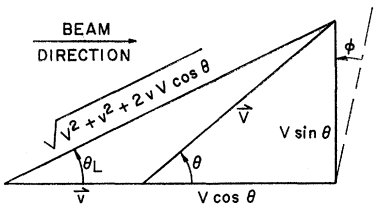

FIG. 4. Diagram of velocity vectors used in fitting the data for $v_\perp=0$. The velocity imparted in the initial phase of the reaction is given by **v**, in the second phase by **V**. The resulting direction of recoil in the laboratory system is given by the angle θ_L. In the system of the struck nucleus the corresponding angle is θ. The angle by which the vector **v**+**V** is rotated around the beam direction is ϕ. This vector is labeled by its absolute value $(V^2+v^2+2vV\cos\theta)^{1/2}$.

In the experiment as performed here, this velocity is not measured directly. Instead, the forward and perpendicular projections of the recoil range in Al are the quantities measured. The recoil ranges of Tb^{149} in Al have been determined for kinetic energies between 4 and 29 MeV.[7,9] Hence, it is possible to deduce the velocity (or kinetic-energy) distribution from the range distribution.

The relation between the range and the recoil velocity can be conveniently expressed as

$$\text{range}=k|\mathbf{v}+\mathbf{V}|^N. \tag{1}$$

Over a restricted region of recoil velocities, k and N are constants.

1. The Distribution in the Values of V

The experimental results are analyzed in terms of the proposed model in order to determine the values of v and V. The distribution in the values of V can be surmised from the experiments at the proton bombarding energies greater than several BeV. At these energies the momentum transfer, and hence the velocity v, are small (Table IV). As a result, the experimentally observed projected range distribution approaches isotropy as the bombarding energy increases.

This permits us to analyze the experimental results at the highest incident proton energies to obtain the distribution in the values of $R=kV^N$, the ranges of Tb^{149} in Al from the second phase of the reaction. The distribution in the values of V and the corresponding kinetic energy, $E=\frac{1}{2}MV^2$, can be obtained from these values of R. Here, M=mass of the Tb^{149} atom.

In order to see how this analysis was made, consider the simple case of a point source of recoiling radioactive atoms, all having the same range R in foils of uniform thickness placed around the source [Fig. 5(a)]. The points at which the recoiling atoms come to rest define a sphere of radius R. (The effect of range straggling will be discussed later.) Now, it is the property of a sphere that parallel planes separated by a given distance divide the total spherical surface into segments of equal area. Hence, all foils that are within a distance R of the source

[7] L. Winsberg and J. M. Alexander, Phys. Rev. **121**, 518 (1961).
[8] D. Bodansky, Ann. Rev. Nucl. Sci. **12**, 79 (1962).
[9] J. M. Alexander and D. H. Sisson, Phys. Rev. **128**, 2288 (1962).
[10] N. Sugarman, M. Campos, and K. Wielgoz, Phys. Rev. **101**, 388 (1956).
[11] E. R. Merz and A. A. Caretto, Phys. Rev. **126**, 1173 (1962).
[12] A. M. Poskanzer, J. B. Cumming, and R. L. Wolfgang, Phys. Rev. **129**, 374 (1963).
[13] W. R. Pierson and N. Sugarman, Phys. Rev. **130**, 2417 (1963).

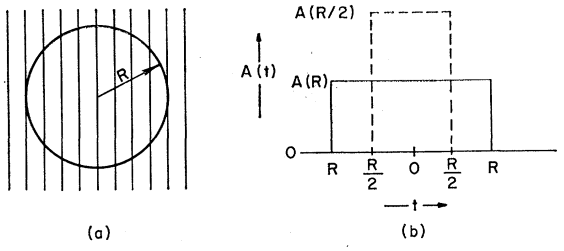

FIG. 5. Distribution of atoms recoiling isotropically with a given range. (a) Atoms that recoil with a range R are distributed on the surface of a sphere of radius R. In this diagram the parallel lines represent the interfaces of foils of uniform thickness with the source at the center interface. (b) The distribution of activity $A(t)$ in each foil, arranged as in part (a) of this figure, is shown here. The solid line represents this distribution for atoms with the range R, the dashed line for the range $R/2$. The thickness of absorber is given by t.

will contain the same number of stopped atoms. Foils located at a distance greater than R will contain no stopped atoms. The resulting activity distribution $A(R)$ is shown by the solid line in Fig. 5(b).

If, in addition, the source emits a second group of atoms of the same activity as the first, but having the range $R/2$, we will obtain the distribution shown as a dashed line in Fig. 5(b). Clearly, the activity of each group of atoms per unit thickness of foil is inversely proportional to its range.

Therefore, in the isotropic case

$$A(R_i)=\text{constant}\ P(R_i)/R_i \tag{2}$$

at distances smaller than R_i from the source. Here, $A(R_i)$ is the activity per unit foil thickness of atoms of range R_i and $P(R_i)$ is the relative probability per unit range to have atoms of the range R_i.

The total activity at the distance t is given by

$$A(t)=\sum_i A(R_i)=\text{constant}\sum_i P(R_i)/R_i, \tag{3}$$

where $A(R_i)$ and $P(R_i)/R_i$ are summed over all values of $R_i>t$. For a continuous distribution of ranges

$$A(t)=\text{constant}\int_t^\infty \frac{P(R)}{R}dR. \tag{4}$$

The experimentally determined distribution of the Tb^{149} recoil activity as a function of t is given in Fig. 3 for two typical cases. This distribution is essentially exponential for all projections (forward, backward, and perpendicular) of the proton-induced recoils at all energies studied. [The same is true for the alpha-particle bombardments (Fig. 3), except for the forward projections. The latter exception is due to the large momentum transfer, and hence large v, in these cases.]

Thus, we take

$$\int_t^\infty \frac{P(R)}{R}dR=\text{constant}\ e^{-\text{constant}\ t} \tag{5}$$

or

$$P(R)dR=(4R/\bar{R}^2)\exp(-2R/\bar{R})dR, \tag{6}$$

where $P(R)dR$, which is properly normalized, represents the distribution of ranges of recoils from the second (isotropic) phase of the reaction. The mean range is given by $\bar{R}$.

The corresponding distribution in the values of E can be obtained since $R=f(E)$ is known for Tb^{149} stopping in aluminum.[7,9] For recoil energies below 7 MeV, R is proportional to E, i.e., $R=kV^N$, where $N=2$. Thus, the distribution in E is given by

$$P(E)dE=(4E/\bar{E}^2)\exp(-2E/\bar{E})dE, \tag{7}$$

where $\bar{E}$ is the mean recoil energy in the isotropic phase of the reaction.

At recoil energies above 7 MeV the value of N decreases gradually. However, both this effect and the effect of range straggling are too small to change the form of Eq. (6) or (7).

It is interesting to observe that the exponential nature of the distribution of projected recoil distances persists even for cases where the momentum transfer from the first phase of the reaction is large, i.e., for $v\gg 0$ (Tables IV, X, Fig. 3).

The effect of v appears in two ways: (1) More atoms recoil in the forward direction compared to the backward direction. (2) The average projected forward range is larger than the average projected backward range. Both effects decrease as the energy of the bombarding particle increases.

2. The Over-All Calculation and the Distribution in the Values of v

The complete analysis of the recoil results was based on the distribution of E (and V) given by Eq. (7). The distribution in the values of v, the velocity imparted in the first part of the reaction, was determined by comparing the thin target recoil distributions (Fig. 3) with a machine (IBM-704) computation.

The procedure followed was to compute synthetic results with several values of the parameters that appear in the calculation. The synthetic and experimental results were then compared. The set of parameters that give the best fit establishes the distribution in v and, therefore, the momentum transfer in the first stage of the reaction and also the value for $\bar{E}$, the average recoil energy in the second stage of the reaction [see Eq. (7)].

At first the effect of range straggling was disregarded. This effect was included in the final computation.

The steps in the initial computation were as follows:

(1) Equations (6) and (7) become

$$P(X)dX=Xe^{-X}dX \tag{8}$$

if we take

$$X=2R/\bar{R}=2E/\bar{E}. \tag{9}$$

A set of j values of X that have the distribution given

by Eq. (8) was obtained by solving

$$\int_{X_i}^{\infty} P(X)dX=(X_i+1)e^{-X_i}=(i-\tfrac{1}{2})/j, \quad (10)$$

for X_i by Newton's method. The values of i are 1, 2, 3, $\cdots$, j. The value of j was usually taken to be 25. Larger values of j required a prohibitive amount of computer time for the total calculation without improving the accuracy of the results appreciably.

(2) A functional relationship between v and E of the form

$$v/V=\text{constant}/E^n=(a/X)^n \quad (11)$$

was assumed, where a and n are constants, and X is given by Eq. (9). The value of a is fixed by the assigned value of n and by the experimental value of $B(0)$, the fraction of Tb^{149} atoms that recoils backward out of a zero-thickness target. Since the total activity is normalized to unity,

$$B(0)=1-F(0), \quad (12)$$

where $F(0)$ is the fraction of atoms that recoils forward.

For a given value of v/V, we have (see Fig. 4)

$$B(0)=\tfrac{1}{2}\int_{\arccos(-v/V)}^{\pi}\sin\theta d\theta=\tfrac{1}{2}(1-v/V). \quad (13)$$

For any value of $v/V\geqslant 1$, $B(0)=0$.

For a continuous distribution in values of v/V, we have

$$\begin{aligned}B(0)&=\tfrac{1}{2}\int_{v}^{\infty}(1-v/V)P(V)dV\\&=\tfrac{1}{2}\int_{a}^{\infty}[1-(a/X)^n]Xe^{-X}dX\\&=\tfrac{1}{2}(1+a)e^{-a}-\tfrac{1}{2}a^n\Gamma(2-n,a), \quad (14)\end{aligned}$$

where the solution of the gamma function,

$$\Gamma(2-n,a)=\int_{a}^{\infty}e^{-X}X^{1-n}dX,$$

is given by a FORTRAN subroutine.

Equation (14) was solved for a by Newton's method for several values of n between 0 and 1, and for each experimental value of $B(0)$.

(3) The range of an atom recoiling at an angle θ_L to the direction of the incident particle is given by (see Fig. 4)

$$\begin{aligned}\mathfrak{R}_0&=k|\mathbf{v}+\mathbf{V}|^N, \quad (15)\\&=k(V^2+v^2+2vV\cos\theta)^{N/2}, \quad (16)\\&=k[(\bar{E}/M)X(1+v^2/V^2+2(v/V)\cos\theta)]^{N/2}, \quad (17)\end{aligned}$$

where v/V is given by Eq. (11). The angle between $\mathbf{V}$ and $\mathbf{v}$ is given by θ. In this case the direction of $\mathbf{v}$ coincides with the forward direction.

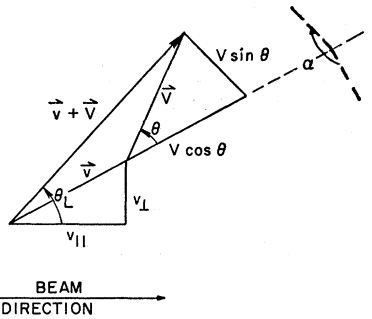

FIG. 6. Diagram of velocity vectors used in fitting the data for $v_\perp\neq 0$. The angle between the $v_{||}-v_\perp$ plane and the plane containing $\mathbf{V}$ and $(\mathbf{v}+\mathbf{V})$ is α. The forward component of $\mathbf{v}$ is given by $v_{||}$, the perpendicular component by $v_\perp$. The other quantities are defined under Fig. 4. For clarity the angle ϕ is not shown here.

We define S_0 by the quantity

$$\begin{aligned}S_0&=\mathfrak{R}_0/k(\bar{E}/M)^{N/2}\\&=[X(1+v^2/V^2+2(v/V)\cos\theta)]^{N/2}. \quad (18)\end{aligned}$$

The projection of S_0 on the forward direction is given by

$$S_F=S_0\cos\theta_L, \quad (19)$$

where

$$\cos\theta_L=(v/V+\cos\theta)/(1+v^2/V^2+2(v/V)\cos\theta)^{1/2}. \quad (20)$$

Negative values from Eq. (19) were assigned to S_B, the corresponding quantity for the backward direction.

Similarly, for the projection of S_0 on a given perpendicular direction we have

$$S_P=S_0\sin\theta_L\cos\phi, \quad (21)$$

where ϕ is the angle between $V\sin\theta$ in Fig. 4 and this perpendicular direction. The angle ϕ varies uniformly from 0 to 2π, and

$$\sin\theta_L=\sin\theta/(1+v^2/V^2+2(v/V)\cos\theta)^{1/2}. \quad (22)$$

(4) The calculation was modified to take into account the possibility that $\mathbf{v}$ is not directed along the original beam direction (Fig. 6). In this case there will be a perpendicular component $v_\perp$ in addition to the parallel component $v_{||}$, where

$$v_{||}/V=(a/X)^n. \quad (23)$$

Thus,

$$v=(v_{||}^2+v_\perp^2)^{1/2} \quad (24)$$

and $\mathbf{v}$ is no longer in the forward direction. When $v_\perp=0$, Eqs. (23) and (11) are identical.

Equations (19) and (21) are still valid for this case with θ_L given by

$$\begin{aligned}\cos\theta_L&=(v/V+\cos\theta+C\sin\theta\cos\alpha)/\\&\quad[(1+v^2/V^2+2(v/V)\cos\theta)(1+C^2)]^{1/2}, \quad (25)\end{aligned}$$

where

$$C=v_\perp/v_{||} \quad (26)$$

and α is the angle between the plane containing v_{II}, $v_{\perp}$, and $\mathbf{v}$, and the plane containing $\mathbf{v}$ and $\mathbf{V}$. The angle α varies uniformly between 0 and 2π.

The parameter C was usually given a constant value between 0 and 2. In a few cases the value of C was varied with X according to the relation

$$C=\text{constant}X^c, \tag{27}$$

where c is another constant. The values of v and $\bar{E}$ did not depend significantly on the values of C that gave good fits.

(5) The final distribution of projected ranges depends on the distribution of the angle θ. This angular distribution was taken to be isotropic.

Values of S_F, S_B, and S_P were computed for the spectrum of X values initially calculated and for uniform distributions in $\cos\theta$, in ϕ and (for $C\neq 0$) in α. The final normalized projected range distributions were then compared with the corresponding experimental results. A typical comparison is shown in Fig. 7. The ordinate gives the sum of the activities in the foils located at a thickness greater than t (the abscissa) from the target foil.

In all of the results given here, the value of N in Eqs. (15)–(18) was taken to be 2.0. Since this value of N is valid for the shorter ranges, it is this region that was weighted most in fitting the synthetic results to the experimental results.

3. The Effect of Scattering

The analysis results in the determination of $\bar{R}$, n, and C. In addition, the value of the parameter a is given by Eq. (14). The final values of interest are those for $\bar{E}$, p_{II}, and p_{II}/p_{CN}. In order to get accurate values for these quantities, it is necessary to correct for the effect of the scattering of the Tb^{149} recoiling atoms in aluminum.

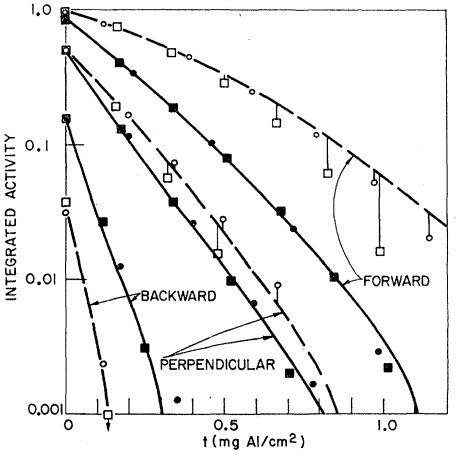

FIG. 7. Comparison of the computer results (dashed and solid lines) with the experimental data at 700 MeV for alpha particles (open points) and protons (closed points) incident on Ta^{181}. The results of this comparison are listed in Tables II–V. The different symbols used in the diagram represent independent experiments. The integrated activity is the sum of the activities in the foils located at a thickness greater than t from the target foil. The total activity is normalized to unity.

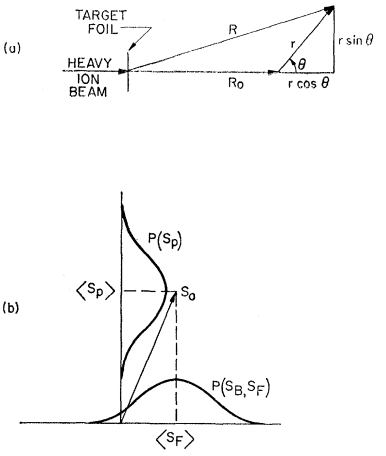

FIG. 8. Diagrams illustrating the effect of scattering in the stopping material. (a) The recoiling atom is assumed to move initially in the beam direction. The distance of recoil is R. The average projected range is R_0. The effect of scattering (and the nuclear reaction) is given by the isotropic quantity r, which is the vector difference between R and R_0. The angle θ defines the direction of r. (b) The recoiling atom is moving in some arbitrary direction. The normalized ranges, S_0, S_B, S_F, and S_P are defined by Eqs. (18), (35), and (36). The distributions of the projected values are given by the curves marked $P(S_B,S_F)$ and $P(S_P)$. The average projection in the forward direction is $\langle S_F\rangle$ in the perpendicular direction $\langle S_P\rangle$ [given by Eqs. (19) and (21), respectively].

The effect of scattering appears in two ways: the distortion of the experimentally observed distribution of recoiling nuclei, and the error introduced into the range-energy curve used in getting $\bar{E}$ from $\bar{R}$. The latter effect will be considered first.

The range-energy curve. The range of Tb^{149} in Al as a function of its recoil energy E has previously been determined by bombarding a suitable target with heavy ions, e.g., C^{12}, N^{14}, O^{16}, etc.[7,9] As a result of the nuclear reaction, the Tb^{149} nucleus recoils a distance R, see Fig. 8(a). Ordinarily, the direction of recoil does not coincide with that of the incident beam because of the nuclear reaction and, more important, because of scattering during the stopping process.

Actually, R_{proj}, the projection of R on the forward direction, was measured. The average value of R_{proj} is given by the expression, $R_0(\mu\text{g Al/cm}^2)=81.2\,E$ (MeV), for $E<7$ MeV. The value for the constant of proportionality was obtained by least-squares analysis of the range data. The distribution of R_{proj} was found to be Gaussian. The width of the Gaussian curve is given by the straggling parameter ρ, where

$$\rho^2=\langle(R_{\text{proj}}-R_0)^2\rangle/R_0^2. \tag{28}$$

The curves reported in the literature are those of R_0 versus E. On the other hand, the experiments reported here are analyzed in terms of R. The effect of

scattering is given by r, the vector difference between R and R_0. Thus,

$$R=(R_0^2+r^2+2rR_0\cos\theta)^{1/2} \tag{29}$$

and

$$R_{\text{proj}}=R_0+r\cos\theta. \tag{30}$$

We assume that r is isotropic and has a Gaussian distribution $P(r)dr$ that will yield the observed distribution in R_{proj}.

The average value of R corresponding to a given value of R_0 is thus

$$\begin{aligned}\bar{R}&=\tfrac{1}{2}\int_0^\infty\int_0^\pi (R_0^2+r^2+2rR_0\cos\theta)^{1/2}\sin\theta d\theta P(r)dr\\&=(1+\rho^2)R_0\\&=1.07\,R_0,\end{aligned} \tag{31}$$

where the value of $\rho=0.26$ is given in Refs. 7 and 9. The value of $\bar{E}$ was read from the range-energy curve at the value of $R_0=\bar{R}/1.07$.

The recoil distribution. In the initial computation, an atom that recoiled with a given velocity in a given direction had a single value for S_0 and for its projections, S_F (or S_B) and S_P. As a result of scattering in the Al stopping foils, each case actually has many values for each of these quantities, distributed in Gaussian fashion around the values initially computed. The distributions of the projected values are shown in Fig. 8(b) as the curves marked $P(S_B,S_F)$ and $P(S_P)$. These curves, as well as $P(S)$, the distribution (not shown here) of the unprojected values S around S_0, have identical shapes as a result of the assumption that the scattering is isotropic about the mean range.

This effect was incorporated into the computation in the following way: The Gaussian distribution of ranges $\mathfrak{R}$, and hence S, is given by

$$P(x)dx=(1/\sqrt{\pi})e^{-x^2}dx, \tag{32}$$

where

$$x=\frac{1}{\sqrt{2}\rho}(\mathfrak{R}/\mathfrak{R}_0-1)=\frac{1}{\sqrt{2}\rho}(S/S_0-1). \tag{33}$$

A set of $2j$ values of x that have the distribution given by Eq. (32) was obtained by solving

$$\frac{2}{\sqrt{\pi}}\int_0^{x_i}e^{-x^2}dx=(i-\tfrac{1}{2})/j \tag{34}$$

for $\pm x_i$ by Newton's method. The value of j was taken to be 10 for most cases. In a few cases j was taken to be 100. A small correction was made for the sensitivity of the results to the value of j.

The value of $(S-S_0)/S_0$ was obtained for each value of x_i from Eq. (33). Thus, we have the values of S_F and S_P given by

$$S_F=S_0(\cos\theta_L\pm\sqrt{2}\rho x_i) \tag{35}$$

and

$$S_P=S_0|\sin\theta_L\cos\phi\pm\sqrt{2}\rho x_i|. \tag{36}$$

Negative values from Eq. (35) were assigned to S_B. The value assigned to S_P was always taken to be positive. As before, $\rho=0.26$.

As a result of scattering, the value of $B(0)$, designated output $B(0)$, that finally results from the computation no longer agrees with the value assigned to $B(0)$ in Eq. (14), i.e., the input $B(0)$. Therefore, the value of the input $B(0)$ was varied until the output $B(0)$ agreed with the experimental value.

The computation with scattering included (designated $\rho=0.26$) gives agreement with the experimental results similar to the comparison shown in Fig. 7. The parameters that give agreement in this case, however, are different from those obtained in the initial ($\rho=0$) computation.

RESULTS

The cross sections (in mb) for the formation of Tb^{149g} from Ta, Au, and Bi are given in Table I and Fig. 9.

TABLE I. Cross sections (mb) for the formation of Tb^{149} as a function of bombarding energy T.

T(BeV)	Ta^{181}	Au^{197}	Bi^{209}
	Alpha-particle bombardments		
0.50	5.7	0.06	
0.70	16.5	0.93	
0.88	20.0	3.9	
	Proton bombardments		
0.45	2.8[a] 4.1[b]		
0.60	9.5	0.3	
0.70	14.5	1.2	
1.0	18.8	7.5	2.2
1.3	18.7	11.9	5.1
1.7	15.4	15.2	9.1
2.0	13.0	14.9	10.6
2.5	11.2	12.5	10.5
3.0	10.7	12.5	10.6
3.2	10.5	12.2	10.5
4.0	9.2	10.5	9.0
4.5	8.5	10.2	9.1
5.0	8.5	9.6	8.7
6.2	7.9	8.7	8.0

[a] Bombardment was performed at 184-in. cyclotron. Nominal energy was 450 MeV. Actual energy was probably closer to 400 MeV.
[b] Bombardment was performed at Fermi Institute cyclotron. Nominal energy was 450 MeV. Average energy was actually ~420 MeV.

These values have been corrected for counting efficiency and for the alpha branching ratio, and include any contribution from the excited state of Tb^{149} by isomeric transition to Tb^{149g}. Other measurements of these cross sections were made by Duffield, Friedlander, and Miller. Their values for gold are reported in Ref. 5.

The data from the thin-target experiments are tabulated in the Appendix. The results of the analysis of this information in the manner described above, as based on the final ($\rho=0.26$) computation, are given in Tables II–V. The experimental values of $B(0)$ are given in

TABLE II. Values of the parameters n and $a^{0.5}$ [Eqs. (11) and (23)] and C [Eqs. (26) and (27)].

T	Ta^{181}			Au^{197}			Bi^{209}		
(BeV)	n	$a^{0.5}$	C	n	$a^{0.5}$	C	n	$a^{0.5}$	C
				Alpha-particle bombardments					
0.50	0.5–0.75	1.559	0						
0.70	0.5	1.559	0	0.5	1.143	0			
0.88	0.5	1.504	0	0.5	1.279	0			
			$\langle C^2\rangle=0$			$\langle C^2\rangle=0$			
				Proton bombardments					
0.45	0.5	0.991	0.5						
0.70	0.5	0.874	$0.25X^{0.5}$	0.5	0.737	0			
1.0	0.5	0.720	0	0.5	0.671	1.0			
1.7				0.5	0.641				
3.0	0.5	0.461	1.0	0.75	0.537	1.0	0.5–0.75	0.477	0
4.5				0.5	0.432				
6.2	0.5–0.75	0.390	$1.0X^{0.5}$	0.5	0.413	0	0.5	0.376	0
			$\langle C^2\rangle=0.6$			$\langle C^2\rangle=0.5$			$\langle C^2\rangle=0$

Table III (and in the Appendix). The parameters that result from the comparison of the computed and experimental results are n, a, C, (see Table II), and $\bar{E}$ (see Table IV). The information about the kinetics of the reaction is derived from the values of these parameters and is given in Tables III–V.

TABLE III. Values of $B(0)$ and $\langle v_{II}/V\rangle$.

T	Ta^{181}		Au^{197}		Bi^{209}	
(BeV)	$B(0)$	$\langle v_{II}/V\rangle$	$B(0)$	$\langle v_{II}/V\rangle$	$B(0)$	$\langle v_{II}/V\rangle$
			Alpha-particle bombardments			
0.50	0.036	1.38				
0.70	0.036	1.38	0.098	1.01		
0.88	0.041	1.33	0.072	1.13		
			Proton bombardments			
0.45	0.134	0.88				
0.70	0.166	0.77	0.210	0.65		
1.0	0.216	0.64	0.233	0.59		
1.7			0.244	0.57		
3.0	0.311	0.41	0.282	0.48	0.305	0.42
4.5			0.323	0.38		
6.2	0.340	0.35	0.332	0.37	0.346	0.33

The values of the parameters n and C that give the best fit are given in Table II. For most cases the value of n was found to be 0.5. This result has an interesting interpretation. According to Eqs. (9), (11), and (23),

$$v_{II}=V \text{ constant}/E^{0.5}. \tag{37}$$

Thus, v_{II} is a constant since $E^{0.5}=(M/2)^{1/2}V$. In other words, the momentum transfer given by mv_{II} is a constant at each combination of projectile, bombardment energy, and target nucleus.

The values of C that best fit the experimental data are given in Table II. The nonzero values of C were required in order to fit the perpendicular recoil projections in the cases indicated. No attempt was made to establish precise values of C. The values $C=0$ and $n=0.5$ were used to obtain all the entries listed for $a^{0.5}$, $\langle v_{II}/V\rangle$, $\bar{E}$, p_{II}, and p_{II}/p_{CN} in Tables II–V. These four quantities were insensitive to C. The quantity $\langle v_{II}/V\rangle$ is given by

$$\langle v_{II}/V\rangle=\int_0^\infty (a/X)^{1/2}Xe^{-X}dX=\tfrac{1}{2}(\pi a)^{1/2} \tag{38}$$

TABLE IV. Recoil properties of Tb^{149}.

T	Ta^{181}			Au^{197}			Bi^{209}		
(BeV)	$\bar{E}$ (MeV)	p_{II} (MeV/c)	p_{II}/p_{CN}	$\bar{E}$ (MeV)	p_{II} (MeV/c)	p_{II}/p_{CN}	$\bar{E}$ (MeV)	p_{II} (MeV/c)	p_{II}/p_{CN}
				Alpha-particle bombardments					
0.50	~2.5	~1130	~0.57						
0.70	2.5	1130	0.48	~4.4	~1190	~0.51			
0.88	2.5	1090	0.41	~4.6	~1360	~0.51			
	2.5			4.5±0.1					
				Proton bombardments					
0.45	2.15	660	0.65						
0.70	2.5	630	0.47	3.9	720	0.54			
1.0	2.6	530	0.31	3.8	640	0.38			
1.7				4.2	650	0.27			
3.0	2.8	350	0.093	3.7	510	0.13	4.8	550	0.14
4.5				3.6	400	0.076			
6.2	2.5	280	0.040	4.0	400	0.058	4.9	440	0.062
	2.5±0.1			3.9±0.2			4.9±0.1		

TABLE V. Values of p_{II}/p_{CN} for proton and alpha-particle bombardments.

T (BeV)	Ta^{181} Proton	Ta^{181} Alpha	Au^{197} Proton	Au^{197} Alpha
0.45	0.65			
0.50	0.61[a]	~0.57		
0.70	0.47	0.48	0.54	~0.51
0.88	0.37[a]	0.41	0.44[a]	~0.51
1.00	0.31		0.38	

[a] These values were obtained by graphical interpolation.

for $n=0.5$, see Eqs. (8), (11), and (23). These values are listed in Table III along with the experimental values of $B(0)$. For cases in which all values of v_{II}/V are less than unity, we get from Eq. (13)

$$B(0)=\tfrac{1}{2}(1-\langle v_{II}/V\rangle) \quad (39)$$

if scattering does not occur. The results of the initial ($\rho=0$) computation agree with Eq. (39) for the cases where $\langle v_{II}/V\rangle \ll 1$. The effect of scattering, however, causes the value of $B(0)$ calculated from Eq. (39) to be low by approximately 5% for these cases, see Table III.

The value of $\bar{E}$ was insensitive to the value of n for the cases where the momentum transfer p was small. However, this is not true of the alpha-particle-induced reactions. Here, the momentum transfer is large, and the results were, therefore, found to be sensitive to the value of n. For this reason and because the large-range values are no longer strictly proportional to the kinetic energy, these values of $\bar{E}$ are most likely to be in error.

The values of p_{II} and p_{II}/p_{CN} given in Table IV are based on the values for $a^{0.5}$ from Table II, and $\bar{E}$ from Table IV. With Eqs. (9), (11), and (23) we have

$$p_{II}=mV(a/X)^{1/2}=(931aA^2\bar{E}/149)^{1/2}\ \mathrm{MeV}/c, \quad (40)$$

where m is the mass and A is the mass number of the intermediate nucleus that recoils with the velocity v. Equations (37) and (40) are, of course, equivalent. The value of A was taken to be the mass number of the target nucleus for the proton bombardments and 2 units greater for the alpha-particle bombardments. The reason for these choices is given below.

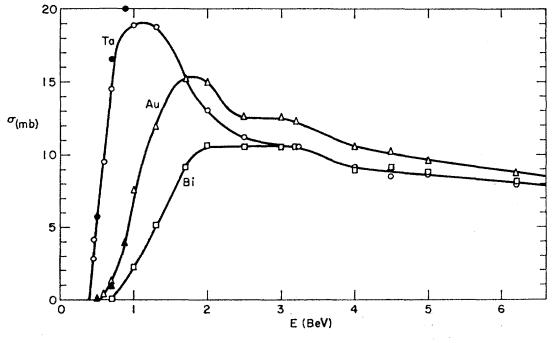

FIG. 9. The excitation functions for the formation of Tb^{149} from proton bombardments of Ta^{181} (○), Au^{197} (△), Bi^{209} (□) and from alpha-particle bombardments of Ta^{181} (●) and Au^{197} (▲). See Table I. The solid lines merely connect the points.

The value of p_{II}/p_{CN} is given by

$$p_{II}/p_{CN}=v_{II}/v_{CN}=[a\bar{E}/931\times 149]^{1/2}/[A_1(\gamma_1^2-1)^{1/2}/(A_1+A_T)], \quad (41)$$

where A_1 and A_T are the mass numbers of the bombarding particle (proton or alpha particle) and the target nucleus, respectively; γ_1 is equal to the total relativistic energy of the bombarding particle divided by its rest mass energy. In obtaining Eq. (41), v_{CN} was taken to be equal to the velocity of the center of mass of the system comprising the projectile and the target. Actually, the two velocities may be different as a result of nuclear evaporation. However, this effect is expected to be small and was, therefore, disregarded. As can be seen from Eq. (41) p_{II}/p_{CN} does not depend on the mass number A of the intermediate nucleus. Furthermore, p_{II}/p_{CN} appears to be the same for proton and alpha-particle bombardments at the same energy, see Table V.

The values of $\bar{E}$ given in Table IV are approximately 10% smaller than the values obtained from the initial ($\rho=0$) calculation. In contrast, essentially the same values of p_{II} and p_{II}/p_{CN} are obtained from the $\rho=0$ and from the $\rho=0.26$ computations. The effect on $\bar{E}$ is reasonable in view of the fact that range scattering adds an extra isotropic component to the initially assumed isotropy in the recoil vectors R. On the other hand, the momentum transfer is expected to be unaffected since it is directed predominantly forward. Because the effect of scattering is small, the final results given in Tables III and IV will be unaffected by the assumed nature of the scattering process.

DISCUSSION

The recoil and cross-section measurements indicate several striking features of the mechanism for producing Tb^{149} from the bombardment of heavy nuclei with protons and alpha particles:

(1) The momentum transfer is constant as indicated by the observation that $n=0.5$ (Table II). Actually, a distribution in the values of p, e.g., of a Gaussian nature, around some average value would give the same result. The recoil measurements are not sufficiently accurate to indicate the nature of the distribution. Thus, the values of p_{II} and p_{II}/p_{CN} given in Table IV are actually average values.

(2) The average momentum transfer p_{II} and the fractional momentum transfer p_{II}/p_{CN} decrease with energy (Table IV).

(3) The fractional momentum transfer p_{II}/p_{CN} for proton-induced reactions is the same within experimental error as that for the alpha-particle induced reactions at the same bombarding energy (Table V).

(4) The distribution of the recoil energies E of Tb^{149} (and its radioactive parents) in the second stage of the

reaction has the form given by Eq. (7) for both proton and alpha-particle bombardments.

(5) For a given target the value of $\bar{E}$ is the same within experimental error, independent of the bombarding energy and projectile (Table IV). The value 2.15 MeV for the interaction of 0.45-BeV protons with Ta^{181} appears to be an exception.

(6) The cross sections for the formation of Tb^{149} with a given target are the same within experimental error for proton and for alpha-particle bombardments at the same energy (Table I and Fig. 9).

(7) The excitation functions for the proton bombardment of Ta and Au rise to a maximum at ~ 1 and ~ 2 BeV, respectively, and then decrease with a further increase in bombarding energy (Table I and Fig. 9). No pronounced maximum is noticeable with Bi as the target. Thus, the peaking in the excitation function decreases with an increase in the mass of the target nucleus.

We see here a marked similarity in the proton and alpha-particle-induced reactions.

The significance of these results becomes apparent if we analyze the data from Tables II and IV in detail. Let us consider the interaction of a particle of mass A_1, kinetic energy T, and momentum P with a nucleus. The initial event will result in a recoil nucleus of mass A (possibly different from that of the target nucleus) moving with a momentum p in the laboratory system and having the excitation energy E^*. The forward component of p is denoted p_{11} as before. As a result of this initial event, one or several other particles will also be present. These may be any combination of neutrons, protons, deuterons, alpha particles, pions, etc. We will treat all these latter particles as a single particle having the mass $A_2+\Delta m$ and the kinetic energy T_2. In this treatment A_2 is the total mass of the nucleons comprising this postulated particle, and Δm is the mass of all pions, kaons, etc., also formed plus the mass equivalent of the binding energies and excitation energies of aggregates of nucleons plus the kinetic energies of all these particles in the center-of-mass system of this single postulated particle. The masses A_1 and A_2 are to be given in units of m_0, the mass of the free nucleon. In this unit A_2 is an integer. For the proton bombardments A_1 is, of course, unity. The objective of this analysis is to determine the values of E^*, A_2, and Δm.

Taking $W=E^*+\Delta m$ and using the units m_0c for momentum and m_0c^2 for energy, we obtain the following relations by applying the laws of energy and momentum conservation:

$$W^2-2(A_2+\Delta m+T)W+2(A_2+\Delta m-A_1)T+2Pp_{11}-p^2=0, \quad (42)$$

or

$$E^{*2}-2(A_2+T)E^*+2(A_2-A_1)T+2Pp_{11}-p^2-2A_2\Delta m-(\Delta m)^2=0. \quad (43)$$

The derivation of Eqs. (42) and (43) is straightforward. The momentum of the postulated particle of mass $A_2+\Delta m$ is given by

$$p_2^2=P^2+p^2-2Pp_{11} \quad (44)$$

from momentum conservation and by

$$p_2^2=T_2^2+2(A_2+\Delta m)T_2 \quad (45)$$

from the relativistic expression relating momentum and energy. From mass-energy conservation we get

$$T_2=T-E^*-\Delta m-T_{\text{recoil}} \cong T-W, \quad (46)$$

where $T_{\text{recoil}}=p^2/2A$ is the kinetic energy of the recoiling nucleus. The value of T_{recoil} is approximately 1 MeV, see Table IV, which is negligible with respect to the other quantities in Eq. (46). By combining Eqs. (44), (45), and (46), we get Eqs. (42) and (43).

The values A_1, T, and P are given by the experiment. The values of p_{11} (see Table IV) were obtained from Eq. (40) with the values of the parameters a and $\bar{E}$ from Tables II and IV, and with the assumed values of A. From Eq. (26), $p_\perp=Cp_{11}$, or $p^2=(1+C^2)p_{11}^2$. The experimental values of C and $\langle C^2\rangle$ are given in Table II. In the alpha-particle bombardments $C^2=0$. The maximum possible value for C^2 consistent with the results of these experiments is 0.1. The values of C obtained from the proton-induced reactions vary appreciably. Most of this variation is undoubtedly due to experimental errors, and to the uncertainties inherent in the analysis of the data. The values of $\langle C^2\rangle$ for these reactions are approximately 0.6 (Ta^{181} target), 0.5 (Au^{197}), and 0 (Bi^{209}) with a large uncertainty.

1. The Proton Bombardments

In the case of the proton bombardments of Ta^{181} and Au^{197}, the values of E^*, A_2, and Δm were determined by the method of least squares.[14] We first assume that A_2 and Δm do not vary over the range of proton energies studied. The constancy of $\bar{E}$ as a function of proton energy (Table IV) indicates that the value of E^* is also constant since the two quantities are directly related. Equation (42) was used here.

The results of this analysis (as well as information from the experiments on Bi^{209}) are given in Table VI. The data from the interaction of 0.45-BeV protons with Ta^{181} are not included in this analysis because of the small value of $\bar{E}$, which indicates that E^* at this energy is smaller than the value at the other energies. However, the results were essentially the same when the data at this energy were included in the analysis. The results obtained with the experimental values of $\langle C^2\rangle$ are italicized. The results with other values of C^2 are included in order to indicate the sensitivity of the final results to this parameter.

[14] W. C. Davidon, Argonne National Laboratory Report ANL-5990 Rev., 1959 (unpublished).

TABLE VI. Values of E^* and Δm in MeV for the proton bombardment[a] of Ta^{181}, Au^{197}, and Bi^{209}. $A_2=1.0$.

	Ta^{181}		Au^{197}		Bi^{209}	
C^2	E^*	Δm	E^*	Δm	E^*	Δm
0	235	305	350	315	*440*	*200*
0.5	245	220	*365*	*200*	470	0
0.6	*250*	*205*	370	175	465	0
1.0	260	130	380	70	455	0
1.26	265	85	390	0	450	0
1.68	275	0				

[a] The values of Δm for Bi^{209} were assigned. The other values of Δm and the values of E^* (all to the nearest 5 MeV) are solutions of Eq. (42). The results based on the experimental values of $\langle C^2\rangle$ from Table II are italicized. The parameter C^2 is defined by Eq. (26).

In all cases A_2 equals unity. This establishes the value of A in Eq. (40) to be equal to the mass of the target nucleus. The value of Δm varies from 0 to approximately 0.3, depending on the value of C^2, whereas the value of E^* varies by less than 10%. The value for E^* given for the target Bi^{209} is the average of the values obtained by means of Eq. (42) at 3.0 and 6.2 BeV (Table IV), with $A_2=$ unity and Δm assigned the value indicated in the table. For $C^2=0$, Δm is the average of the italicized Ta^{181} and Au^{197} values. The other values of Δm were arbitrarily taken to be 0.

The values indicated for E^* are 250 MeV for the target Ta^{181}, 365 MeV for Au^{197}, and 440 MeV for Bi^{209} to an accuracy of about 10%, with $\Delta m=200\pm100$ MeV for all three cases.

These values of E^* are almost identical with the difference between the rest mass of the target nucleus, the rest masses of Tb^{149}, and the remaining nucleons in the unbound state. The latter values are 260 MeV for Ta^{181}, 363 MeV for Au^{197}, and 440 MeV for Bi^{209}. These two sets of similar values indicate that the break up into free nucleons is not possible. The particles emitted in the second phase of the reaction must be sufficiently energetic to cause the observed Tb^{149} recoil energy. No energy is left over for this purpose unless the nucleons are bound into larger particles.

Given the observed values for E^*, $A_2=$ unity, and $C^2=\langle C^2\rangle$ from Table II, we can solve Eq. (43) for Δm at each bombardment energy. The kinetic energy T_2 can be obtained from Eq. (46). The values of T_2 and Δm for the proton bombardments are given in Table VII. These values were also calculated for $E^*=215$ MeV for Ta^{181} at 0.45 BeV. This is the correct value if E^* is proportional to $\bar{E}$, and if $\bar{E}=2.15$ MeV (see Table IV) is correct.

The increase in the values of Δm as the bombarding energy increases to about 3 BeV suggests that the associated mass Δm is due to the formation of pions. The precise values of Δm are not known because of the experimental errors in p_{11} and C^2. However, this trend in the values of Δm is undoubtedly correct and resembles the variation with energy of pion production in free nucleon-nucleon collisions.[15] The decrease in the values of Δm above 3 BeV is probably not significant, since these values are obtained from the difference of relatively large numbers.

TABLE VII. Values of T_2 (BeV) and Δm (to the nearest 5 MeV) for the proton bombardment of Ta^{181}, Au^{197}, and Bi^{209}.

T (BeV)	Ta^{181} ($E^*=250$ MeV, $C^2=0.6$)		Au^{197} ($E^*=365$ MeV, $C^2=0.5$)		Bi^{209} ($E^*=440$ MeV, $C^2=0$)	
	T_2 (BeV)	Δm (MeV)	T_2 (BeV)	Δm (MeV)	T_2 (BeV)	Δm (MeV)
0.45	0.22 0.21	−25 25[a]				
0.70	0.28	170	0.30	35		
1.0	0.51	240	0.48	155		
1.7			0.94	395		
3.0	2.44	305	2.24	390	2.23	330
4.5			4.02	120		
6.2	5.76	185	5.64	190	5.79	−30

[a] Calculated for $E^*=215$ MeV, the correct value if E^* is proportional to $\bar{E}$ and if $\bar{E}=2.15$ MeV (see Table IV).

2. The Alpha-Particle Bombardments

Each alpha-particle bombardment (see Table IV) was also analyzed by means of Eq. (43) in order to determine the values of A_2 and Δm. Since the values of $\bar{E}$ are essentially the same for the proton and for the alpha-particle bombardments, the values for E^* were also taken to be the same, namely 250 MeV for the target Ta^{181} and 365 MeV for Au^{197} (see Tables IV and VI). The value of Δm was also calculated for $E^*(Au^{197})=420$ MeV. This is the correct value if E^* is proportional to $\bar{E}$, and if the average values given in Table IV for $\bar{E}$ are correct.

The resulting values of T_2 and Δm are given in Table VIII for $A_2=2$, 3, and 4, and for $C^2=0$ (see Table II). When $C^2=0.1$, Δm is decreased by approximately 40 MeV for $A_2=2$, by 25 MeV for $A_2=3$, and by 20 MeV for $A_2=4$. The values of Δm for $A_2=1$ are all negative and are, therefore, not included in Table VIII.

The values $A_2\geq2$ are consistent with the experimental results. Because of the limited range of alpha-particle energies available, it is not possible to establish the value of A_2 with certainty. However, the simplest mechanism is obtained if $A_2=2$. For this case Δm is close to zero, and we have a simple (α, 2 nucleon) stripping reaction in which two nucleons are transferred from the alpha particle to the struck nucleus. The remaining two nucleons continue in the initial direction with their velocities essentially unchanged. It is, of course, possible that a variety of processes occur in this first phase of the interaction each with its particular value of A_2 and Δm.

[15] W. O. Lock, *High Energy Nuclear Physics* (Methuen and Company, Ltd., London, 1960), Chap. 8.

TABLE VIII. Values of T_2 and Δm to the nearest 5 MeV for the alpha-particle bombardment of Ta^{181} and Au^{197} for $C^2=0$.

A_2	T (BeV)	Ta^{181} ($E^*=250$ MeV) T_2 (MeV)	Δm (MeV)	Au^{197} ($E^*=365$ MeV) T_2 (MeV)	Δm (MeV)	Au^{197} ($E^*=420$ MeV) T_2 (MeV)	Δm (MeV)
2	0.50	190	60				
	0.70	380	70	365	−30	375	−95
	0.88	610	20	430	85	440	20
			$\langle\Delta m\rangle_{av}=50$		$\langle\Delta m\rangle_{av}=30$		$\langle\Delta m\rangle_{av}=-40$
3	0.50	130	120				
	0.70	260	190	245	90	250	30
	0.88	415	215	295	220	300	160
			$\langle\Delta m\rangle_{av}=175$		$\langle\Delta m\rangle_{av}=155$		$\langle\Delta m\rangle_{av}=95$
4	0.50	100	150				
	0.70	200	250	185	150	190	90
	0.88	315	315	225	290	230	230
			$\langle\Delta m\rangle_{av}=240$		$\langle\Delta m\rangle_{av}=220$		$\langle\Delta m\rangle_{av}=160$

The value assigned to A in Eq. (40) for the alpha-particle experiments is based on $A_2=2$.

SUMMARY

The results of this study on the production of Tb^{149} by high-energy protons and alpha particles are summarized in Table IX. Several features of these reactions are apparent from these results.

If the incident particle is a proton, it is scattered inelastically and has associated with it a mass of 0–400 MeV. This excess mass is probably due to the production of pions which, as in the case of free nucleon-nucleon collisions, increases with the energy of the incident proton. In reactions induced by alpha particles, two or more fast nucleons are scattered in the first stage of the reaction. The simple (α, 2 nucleon) stripping reaction is consistent with the experimental results.

At this stage of the reaction the same fraction of the incident momentum has been transmitted to the target nucleus by the incident particle, whether it be a proton or an alpha particle. In the proton experiments with Ta^{181} and Au^{197}, the recoil momentum may have an appreciable component perpendicular to the direction of the incident particle. This is not the case either for the proton experiments with Bi^{209} or for the alpha-particle experiments.

The remainder of the reaction is treated as though it were isotropic in the frame of reference of the recoiling nucleus. Since the experiments performed here give no information on the time sequence of the various steps in the interaction, it is possible that other particles are emitted along with the fast particles in the first stage of the reaction. In this case two possibilities exist: Either these other particles have relatively small kinetic energy or they are emitted isotropically. In either case,

TABLE IX. Summary of results.

Target nuclues / Incident particle	Ta^{181} Proton	Ta^{181} Alpha	Au^{197} Proton	Au^{197} Alpha	Bi^{209} Proton
A_2	1	$\geqslant 2$	1	$\geqslant 2$	1
Δm(MeV) (see Tables VI–VIII)	0–300	$\geqslant 0$	0–400	$\geqslant 0$	0–300
p_{11}(MeV/c)	Constant for each bombarding energy and incident particle; also see Table IV.				
p_{11}/p_{CN} (see Tables IV and V)	Same for protons and α's.		Same for protons and α's.		
$\langle C^2\rangle$	~0.6	0	~0.5	0	0
E^*(MeV)	250	250	365	365	440
$E^*/(A-149)$[a]	7.8	7.4	7.6	7.3	7.3
$P(E)dE$	$P(E)dE=\exp(-2E/\bar{E})4EdE/\bar{E}^2$				
$\bar{E}$(MeV)	2.5	2.5	3.9	4.5	4.9
σ (see Table I and Fig. 9)	Same for protons and α's.		Same for protons and α's.		

[a] The value of A is taken to be that of the target nucleus for the proton experiments and 2 units greater for the alpha-particle experiments.

they would be included in the isotropic phase of the reaction.

The second phase of the reaction appears to be the same for both the proton and the alpha-particle induced reactions. In either type of reaction, the recoil nucleus must have a certain amount of excitation energy, depending on its mass, in order to decay to Tb^{149}. This excitation energy is 7.5 ± 0.3 MeV for each nucleon emitted in the second phase. The distribution of recoil energies of the final mass 149 nucleus in the moving frame of reference is given by Eq. (7). The average recoil energy is several MeV. The latter value and the values of the excitation energy rule out the possibility that the second phase of the reaction consists merely of the emission of unbound nucleons.

Despite some marked differences in the first phase of the reaction, the excitation functions with protons and with alpha particles are identical within experimental error over the range of alpha-particle energies studied. Apparently, the value of the cross section is determined primarily by the second phase of these reactions.

The experiments reported here give some insight into the mechanism of nuclear reactions induced by high-energy protons and alpha particles. The method of interpreting the experimental data and the resulting conclusions are undoubtedly valid for a wide variety of nuclear reactions.

ACKNOWLEDGMENTS

I am deeply grateful to the following colleagues for many stimulating discussions of the work presented here: J. M. Alexander, P. A. Benioff, G. Friedlander, E. K. Hyde, J. M. Miller, A. M. Poskanzer, E. P. Steinberg, and N. Sugarman. B. S. Garbow of the Applied Mathematics Division of the Argonne National Laboratory performed the least-squares analysis of the recoil data.

APPENDIX: TABULATION OF EXPERIMENTAL RECOIL DATA

The recoil data, corrected to zero-thickness target, are tabulated in Table X. The values given here are the

TABLE X. The fraction of the Tb^{149} activity recoiling beyond the absorber thickness t. The number in parenthesis is t in μg Al/cm^2.

$\alpha+Ta^{181}\rightarrow Tb^{149}$				$\alpha+Au^{197}\rightarrow Tb^{149}$		
$T=0.50$ BeV	$T=0.70$ BeV		$T=0.88$ BeV	$T=0.70$ BeV		$T=0.88$ BeV
			Backward			
0.036(0)	0.038(0)	0.034(0)	0.041(0)	0.111(0)	0.085(0)	0.072(0)
0.003(113)	0.001(131)	0.002(123)	0.005(106)	0.025(145)	0.012(126)	0.023(120)
			Forward			
0.964(0)	0.962(0)	0.966(0)	0.959(0)	0.889(0)	0.915(0)	0.928(0)
0.848(102)	0.756(161)	0.699(200)	0.785(120)	0.713(190)	0.682(201)	0.791(132)
0.713(207)	0.474(335)	0.453(389)	0.572(264)	0.491(381)	0.463(399)	0.664(256)
0.547(332)	0.290(497)	0.249(585)	0.339(436)	0.303(571)	0.281(606)	0.479(433)
0.218(633)	0.146(662)	0.119(786)	0.166(641)	0.176(766)	0.168(802)	0.313(612)
0.057(932)	0.061(827)	0.052(971)	0.050(901)	0.087(962)	0.089(983)	0.166(871)
	0.016(993)	0.020(1166)	0.018(1105)	0.026(1164)	0.038(1165)	0.093(1069)
						0.039(1266)
			Perpendicular			
0.500(0)	0.500(0)	0.500(0)	0.500(0)	0.500(0)		0.500(0)
0.176(167)	0.194(160)	0.200(170)	0.194(164)	0.175(150)		0.260(175)
0.046(341)	0.057(318)	0.076(341)	0.053(354)	0.050(297)		0.141(339)
0.018(510)	0.016(477)	0.029(500)	0.010(544)			0.067(524)
		0.010(670)				

$p+Ta^{181}\rightarrow Tb^{149}$						
$T=0.45$ BeV		$T=0.70$ BeV		$T=1.0$ BeV	$T=3.0$ BeV	$T=6.2$ BeV
			Backward			
0.124(0)	0.144(0)	0.168(0)	0.164(0)	0.216(0)	0.311(0)	0.340(0)
0.011(140)	0.015(144)	0.027(117)	0.013(172)	0.021(176)	0.051(178)	0.058(176)
0.002(288)	0.003(280)	0.003(251)	0.001(350)		0.010(351)	0.010(360)
					0.002(530)	
			Forward			
0.876(0)	0.856(0)	0.832(0)	0.836(0)	0.784(0)	0.689(0)	0.660(0)
0.464(139)	0.370(198)	0.414(169)	0.342(215)	0.253(263)	0.249(181)	0.244(168)
0.237(279)	0.148(389)	0.193(339)	0.105(460)	0.057(524)	0.093(369)	0.070(344)
0.112(422)	0.052(578)	0.082(507)	0.024(713)	0.016(789)	0.029(569)	0.020(516)
0.050(563)	0.020(757)	0.032(676)	0.003(981)	0.005(1027)	0.009(771)	0.003(706)
0.018(703)	0.005(949)	0.010(848)			0.003(976)	0.001(893)
0.007(842)	0.001(1141)	0.002(1017)				
0.002(983)						
			Perpendicular			
0.500(0)	0.500(0)	0.500(0)	0.500(0)	0.500(0)	0.500(0)	0.500(0)
0.158(150)	0.159(149)	0.130(176)	0.121(202)	0.126(193)	0.139(184)	0.150(168)
0.048(292)	0.051(308)	0.038(342)	0.027(400)	0.030(390)	0.036(378)	0.046(347)
0.014(434)	0.011(477)	0.010(520)	0.007(592)	0.006(586)	0.007(574)	0.014(526)
0.003(573)	0.002(642)	0.002(705)	0.002(776)	0.001(786)		0.005(690)

TABLE X (*continued*)

$p+Au^{197} \rightarrow Tb^{149}$

$T=0.70$ BeV		$T=1.0$ BeV	$T=1.7$ BeV	$T=3.0$ BeV	$T=4.5$ BeV	$T=6.2$ BeV
			Backward			
0.208(0)	0.212(0)	0.233(0)	0.244(0)	0.282(0)	0.323(0)	0.332(0)
0.059(131)	0.059(151)	0.009(235)	0.065(172)	0.093(152)	0.129(159)	0.102(179)
0.020(264)	0.016(313)		0.018(339)	0.028(316)	0.049(318)	0.032(345)
	0.004(475)		0.006(516)	0.009(493)	0.015(510)	0.014(523)
			0.002(685)		0.006(674)	0.004(692)
					0.002(849)	
			Forward			
0.792(0)	0.788(0)	0.767(0)	0.756(0)	0.718(0)	0.677(0)	0.668(0)
0.486(170)	0.392(254)	0.319(282)	0.466(168)	0.370(183)	0.335(164)	0.338(175)
0.280(337)	0.169(518)	0.129(553)	0.271(334)	0.174(373)	0.158(335)	0.179(346)
0.159(503)	0.052(783)	0.034(852)	0.150(505)	0.078(568)	0.071(499)	0.090(517)
0.084(673)	0.012(1045)		0.080(665)	0.031(769)	0.030(668)	0.041(691)
0.047(836)			0.041(835)	0.007(976)	0.012(828)	0.020(855)
0.020(1003)			0.019(1007)		0.005(995)	0.005(1031)
0.006(1171)			0.009(1177)		0.002(1160)	
			0.005(1347)		0.001(1323)	
			0.003(1519)			
			0.001(1713)			
			Perpendicular			
0.500(0)	0.500(0)	0.500(0)		0.500(0)		0.500(0)
0.198(182)	0.189(196)	0.212(210)		0.219(189)		0.203(173)
0.092(362)	0.062(392)	0.049(450)		0.080(374)		0.079(346)
0.034(540)	0.013(590)			0.030(571)		0.028(526)
0.004(718)				0.005(760)		0.008(712)

$p+Bi^{209} \rightarrow Tb^{149}$

$T=3.0$ BeV			$T=6.2$ BeV		
Backward	Forward	Perpendicular	Backward	Forward	Perpendicular
0.305(0)	0.695(0)	0.500(0)	0.346(0)	0.654(0)	0.500(0)
0.122(154)	0.388(199)	0.236(190)	0.131(179)	0.376(168)	0.216(195)
0.041(320)	0.205(403)	0.107(379)	0.056(359)	0.222(341)	0.096(391)
0.014(492)	0.100(606)	0.042(574)	0.028(526)	0.134(515)	0.044(592)
0.004(692)	0.047(811)	0.015(765)	0.008(688)	0.078(682)	0.020(779)
	0.021(1015)		0.004(854)	0.041(854)	0.004(976)
				0.016(1034)	
				0.006(1198)	

sum of Tb^{149} activities beyond t, the thickness of the aluminum absorbers in $\mu g/cm^2$, divided by the total activity. The value of t is given in the parenthesis following each value of the integrated normalized activity. The arrangement of the foils in these experiments is shown in Fig. 1(b). The orientation of the foil stacks with respect to the beam is shown in Fig. 2. In several cases, measurements were repeated at the same bombarding energy. Examples of this are the bombardments at $T=0.70$ BeV.